Available online at www.sciencedirect.com
SCIENCE DIRECT®
Coordination Chemistry Reviews 248 (2004) 1259–1270
COORDINATION CHEMISTRY REVIEWS
www.elsevier.com/locate/ccr

Review

Primary and final charge separation in the nano-structured dye-sensitized electrochemical solar cell

Klaus Schwarzburg, Ralph Ernstorfer, Silke Felber, Frank Willig*

Dynamics of Interfacial Reactions, Department SE4, Hahn-Meitner-Institut, Glienickerstrasse 100, 14109 Berlin, Germany

Received 31 December 2003; accepted 31 December 2003
Available online 22 July 2004

Contents

Abstract

A time constant of 13 fs was measured via transient absorption for electron transfer from the excited singlet state of the chromophore perylene into anatase TiO_2, when the chromophore was bonded to the surface via a carboxyl group. This result suggests that a similarly short time constant should be valid also for primary charge separation from the bipyridyl ligand of the so-called N3 ruthenium dye into anatase TiO_2. The electron transfer time of perylene became much longer, 3.8 ps, at a distance of about 1.3 nm. Laser pulse induced transients of the photocurrent were measured in the Grätzel-cell (G-cell) for illumination firstly through the SnO_2/TiO_2 interface (SE) and secondly through the opposite SnO_2/electrolyte interface (EE). For EE illumination the transient showed two peaks, the first in the μs range and the second in the ms range. For SE illumination only the early peak was observed. The different shapes of EE compared to SE transients were easily modeled employing a time dependent diffusion equation and appropriate boundary conditions. The experimental rise to the early peak occurred faster than corresponds to diffusion controlled final charge separation at the SnO_2/TiO_2 interface if the same diffusion constant was assumed that was valid in the bulk of the nm-structured sponge-type TiO_2/electrolyte layer. The significance of this experimental result for photovoltaic energy conversion of the G-cell is discussed.

Keywords: Solar cell; Photocurrent transients; TiO_2; Modeling; UPS; Perylene; Femtosecond spectroscopy; Electron transfer; Transport

1. Introduction

It is now more than 10 years ago that Grätzel and ÓRegan published their report on a specific nano-structured dye-sensitized electrochemical solar cell with a high solar conversion efficiency approaching 10% [1]. For brevity we refer in the following to this type of solar cell as the Grätzel-cell or G-cell. Since this first report on the G-cell several variants of this cell have been introduced, and the topic has since been very popular in the field of photo-electrochemistry. It has become a research topic also in photovoltaics and has found entry into the textbooks [2]. The unconventional design of the device and the obvious differences to the other solid state solar cells makes this G-cell an interesting object for principal studies. Topics related to its functioning have inspired and continue to inspire research also in other futuristic fields like molecular electronics. Studying the functioning principles of the G-cell has certainly widened the horizon of photovoltaic research. It is clear now after many years of research on the G-cell that it functions after the same basic principles as the other one band gap solar cells [2,3]. The kinetic

* Corresponding author. Tel.: +49 30 80622200; fax:+49 30 80622434.
E-mail address: willig@hmi.de (F. Willig).

0010-8545/$ – see front matter © 2004 Elsevier B.V. All rights reserved.
doi:10.1016/j.ccr.2004.03.027

details are, however, strikingly different in the G-cell [4–6] from the physical processes that are dominant in the current solar cells and those discussed for future highly efficient solid state solar cells [7]. The kinetic processes and their significance for the effective functioning of the G-cell are now basically clear. This does not mean that every detail has been clarified. There are still interesting open questions concerning important kinetic processes in the G-cell. Some of these open questions will be addressed and answered in this paper. It appears now safe to state, however, that no great surprises are expected to surface in the future with respect to the G-cell. On the other hand, there are several indications that the G-cell can still be improved, probably also simplified. It appears difficult at present to postulate that the G-cell can ever reach an efficiency above 25% as already reached with certain solid state versions of a one band gap cell, like c-Si and in particular the GaAs solar cell [8]. In the latter device the achieved solar conversion efficiency is already close to thermodynamic limiting consideration, i.e. in the range of 30%. In an electrochemical cell like the G-cell specific electrochemical activation energies arise for the electron transfer reactions of redox ions, involving the so-called reorganization energies [9], that lead to additional loss mechanisms compared to a solid state device. Whether the G-cell or one of the many variants inspired by its construction principle will be successful in a practical market will depend on whether one can find the right combination of production costs, solar conversion efficiency, and long time stability. The latter practical issues are not the topic of the present paper. It is devoted to new experimental results and consequences derived from the latter for understanding the detailed functioning of the G-cell.

The processes of light harvesting, primary charge separation, and final charge separation are realized in the G-cell in rather unique ways that are different from realizations of these processes in other photovoltaic cells, i.e. solid state p–n-junction solar cells and hetero-junction solar cells. The G-cell functions also rather differently than the photosynthetic apparatus in bacteria and plants. Incoming light sees in the G-cell many consecutive monomolecular layers of a suitable chromophore such that absorption reaches 100% almost at every wavelength throughout the visible spectrum. The chromophore is anchored on the surface of the transparent wide band gap semiconductor TiO_2 usually with an anchor group like carboxylic acid [1]. For accommodating the monomolecular layers of the chromophore TiO_2 nano-particles form a sponge-type layer structure whose voids provide for a huge inner surface [10]. Unlike in the antenna system of the photosynthetic apparatus there is no energy transfer between the chromophores in a suitably prepared G-cell. The energy of the absorbed photon is immediately utilized in the G-cell for the ultrafast primary charge transfer step. Two product states are formed in less than 20 fs [11], i.e. the electron injected into the TiO_2 nm-particle and the ionized chromophore. The latter represents the hole state. A considerably slower electron transfer step follows where a second electron is transferred from a nearby reduced redox ion to the ionized chromophore [12]. Thereby, the latter returns to its original ground state configuration and is ready for absorbing a new photon. Obviously, for achieving a high photocurrent yield electron uptake from the reduced redox ion must be faster than electron uptake from the TiO_2 nano-particle since the latter process is a recombination reaction that would convert the energy of the absorbed photon completely into heat. In the original version of the G-cell the primary oxidized redox ion undergoes at least two further reaction steps to convert finally to the I_3^- species as the stable form of the oxidized redox ion. For a number of reasons the latter can react only very slowly on the timescale of ms [13] with an electron residing in a nano-particle of TiO_2. This specific electrochemical way of stabilizing spatially separated electron-hole pairs is unique for the G-cell. A surprisingly long recombination time is thus achieved in the range of several ms. The latter value is the prerequisite for efficient final charge separation in the G-cell because the transport of the electrons is very slow through the sponge-like layer formed by the nm-size TiO_2 particles [14,15]. The electrons in the nm-TiO_2 particles are screened by the ions and redox ions in the surrounding electrolyte [4]. Transport of the electrons can be described to a good approximation as diffusion where the parameters like mobility etc. depend on the Quasi-Fermi level and thus on the trap occupancy in the nano-structured material [15]. Recombination with oxidized redox ions is slow but not negligible. The screened electrons can reach the interface with the planar n-SnO_2 electrode that serves as the exit. With the photo-generated electrons entering the planar n-SnO_2 electrode the final charge separation step is realized in the G-cell. The electrons are spatially separated here from the countercharge in the electrolyte, in particular from the oxidized redox ions that function as recombination centers [4]. Obviously, the ions and redox species cannot enter the solid state SnO_2 layer and are left behind in the electrolyte. To achieve high solar energy conversion efficiencies [4,16,17] this final charge separation step requires a driving force, either in the form of a downhill dark potential or in the form of a downhill band offset, where we show below that the dark potential is the better solution.

In this paper, we present new experimental data on the primary femtosecond charge separation and present photocurrent transients and numerical simulations of the latter that shed light on transport of the screened electrons through the nm-structured TiO_2/electrolyte layer and in particular on the final charge separation step in the G-cell.

2. Experimental

Sponge-like nm-structured TiO_2 layers were prepared a few μm thick following the recipe described in the literature [18]. Perylene chromophores were employed to realize a

simple model cases for studying the primary charge separation step. Tertiary-butyl side groups and spacer-cum-anchor groups were covalently attached to the perylene chromophore. The former protected it against dimer formation on the surface and the latter controlled the electron transfer distance and formed via the acid group a stable bond on the surface of TiO_2. The O-atom of the carboxyl group binds to a Ti-atom on the surface of TiO_2 [19]. Among the different anchor-cum-spacer groups investigated in our group we present here results for the short carboxylic group and for a long rigid Tripod structure [20]. For carrying out femtosecond transient absorption measurements the nm-structured TiO_2 layer was prepared on a glass sheet that was less than 100 μm thick. With a thicker glass substrate the initial rise of the measured signal is distorted due to the so-called coherent artifact. Further experimental details concerning the preparation of the nano-structured TiO_2 layer and of the dyes on the latter are described elsewhere [21].

Laser pulses were generated with sub-20 fs autocorrelation width (FWHM) at a repetition rate of 100 kHz for carrying out transient absorption measurements with femtosecond resolution. The wavelength of the laser pulses could be tuned throughout the visible spectral range making use of a novel non-collinear optical parametric amplifier (NOPA) [22]. The latter was added recently to our femtosecond laser system that has been described before [21]. The first excited singlet state of perylene was generated with a pump pulse (20 nJ) of central frequency 430 nm and temporal width of 15 fs (FWHM) [19]. The latter frequency was generated by frequency doubling the near-infrared (NIR) output of the NOPA in a 100 μm thick BBO crystal. Pulse compression was achieved by pre-compensating the NIR pulse with a standard prism compressor. The intensity auto-correlation function of the pump pulse was generated as the 2-photon-absorption signal in a SiC-diode. The much weaker probe pulse was obtained from a white light continuum via spectral filtering and pulse compression in the spectral range of the perylene cation absorption, i.e. centered at 570 nm. The cross-correlation function of pump and probe pulse had a temporal width of 27.6 fs (FWHM). All the transient absorption measurements were carried out with the sample mounted in a UHV chamber with base pressure of 2×10^{-10} mbar.

For measuring photocurrent transients the sponge-like TiO_2 layer was prepared on a different substrate, i.e. a thick sheet of conducting glass (Nippon Sheet Glass) with sheet resistance 8Ω/□. A 40 Å thick Pt layer was sputtered onto the Fluorine doped SnO_2 counter electrode. The thickness of the TiO_2 layer was measured employing Dektak 3030. Heating the TiO_2 layer at 450 °C for 1 h in air removed organic pollutants and improved the surface stoichiometry. Afterwards the sample was transferred into a N_2-purged glovebox. The ruthenium N3 dye [18] was adsorbed at the huge inner surface of the TiO_2 layer by dipping the sample at 50 °C for 2 h into a 10^{-4} M ethanolic solution of the dye. The spatial separation of the working electrode from the counter electrode was achieved by inserting between the two a suitably cut Surlyn 1702 foil (Dupont). The cell was then filled with electrolyte (0.5 M LiI, 0.05 M I_2 in acetonitrile) and was sealed with two-component epoxy glue. The active area of the cell was 0.2 cm^2.

Photocurrent transients were generated in the cell with pump pulses from a Q-switched frequency doubled YAG laser (533 nm excitation wavelength) at a repetition rate of 0.3 Hz. The laser pulse had 15 ns duration (FWHM) and pulse energy of about 1 mJ. The laser pulse was attenuated with several neutral gray density filters before it impinged onto the cell (0.3 cm^2). The laser pulse created photon densities in the range 10^{12} to $10^{15}/cm^2$. By controlling the light intensity the magnitude of the photocurrent transient was kept smaller than 1 mA, typically <100 μA. Thereby, the voltage drop across the series resistance (∼50 Ω) was kept smaller than a few mV. Currents were measured with a home-built current to voltage converter (1 MHz/500 ns rise time) that was connected to a Lecroy 7200 digital oscilloscope. A small fraction of the laser light was fed into a thermopile detector. The signal from the detector was recorded simultaneously with the electrical response from the cell for monitoring and correcting for the fluctuations in the laser pulse intensity. Prior to assembling the cell, absorption spectra (UV–Vis range) were recorded firstly of the TiO_2 layer loaded with dye molecules, secondly of the Fluorine doped SnO_2 conducting glass substrate, and thirdly of the platinized counter electrode cut from the same material. The number of absorbed photons was calculated for the two alternative directions from where the laser beam was impinging onto the sample, i.e. firstly through the SnO_2/TiO_2 interface (SE) and secondly through the opposite SnO_2/electrolyte interface (EE). The nomenclature follows here that in [14]. In calculating the number of photons absorbed by the dye molecules we took into account absorption and reflection of the light by the assembled cell in the absence of the dye and the energy of the respective laser pulse.

3. Primary charge separation in the G-cell

Primary charge separation occurs in the G-cell via electron transfer from the excited state of the adsorbed chromophore into the adjacent nm-size TiO_2 particle that is part of the sponge type layer. Since the latter is structured like a maze all directions in space are equally represented for the vectors connecting the injected electrons with the left behind ionized chromophores. Thus, primary electron transfer leads to a local separation of electrons from the positive charges but there is no macroscopic photopotential connected with primary charge separation in the G-cell. It is an experimental fact that one of the most efficient versions of the G-cell has been achieved with the so-called N3 ruthenium dye as absorber for the impinging sunlight [18]. When considering firstly the chemical structure, secondly the possible configurations

of the anchored N3 dye on the TiO_2 surface, and thirdly the dynamics of the excited electronic states for this dye, it becomes clear that electron injection from the excited state of this dye can be a very complicated process involving several different time constants. The N3 dye has two bipyridyl ligands where only one of them is bonded to the semiconductor with the other staying at a larger distance. Thus, there could be two different time constants for injection of an electron localized on either the closer or on the more distant bipyridil ligand with respect to the TiO_2 surface. The N3 dye has a higher and lower excited state, addressed simply as singlet and triplet state. Energy relaxation from the higher to the lower excited state can occur extremely fast with time constant of a few ten fs [23]. To our knowledge it is not totally clear yet whether upon photon absorption the electron is initially delocalized over both the bipyridyl ligands or is localized on only one of them [24]. Constructing different possible scenarios from the information listed above it is easy to see that more than five different time constants could influence the photo-induced electron injection process. Such a complicated situation can arise if injection from the higher excited state occurs on a time scale comparable with localization of the electron on one of the bipyridil ligands and if conversion to the lower excited state competes with electron transfer, and finally if an electron can also be injected from the lower excited state [23]. Early measurements of our group showed that electrons are injected into TiO_2 from the N3 dye within 20 fs [11]. The complete picture with all the different possible time constants has not yet been unraveled for this system. Some of the data published on electron injection with the N3 dye cannot be easily reconciled with experimental data obtained with the chromophore perylene where electron injection occurs only from the excited singlet state. As will be shown below in the latter case the energy levels are located such that the electron on the molecular donor orbital can utilize many unoccupied electronic states with different energies in the conduction band of TiO_2 and the complete set of Franck-Condon factors of the electron transfer reaction can be accommodated in parallel [25]. Experiments carried out with the chromophore perylene reveal the principal factors governing the injection dynamics of a dye bonded to the surface of a semiconductor. Two very different injection times will be shown below in Figs. 1 and 3 for two different distances of the chromophore perylene from the surface of TiO_2 but for the same orientation of the chromophore with respect to the surface.

Fig. 1 shows the rise of the ionized state of the chromophore perylene upon exciting this chromophore to the first excited state with a 15 fs laser pulse. The chromophores were anchored via a covalently attached carboxylic group on the surface of anatase nm-particles that form the sponge-like TiO_2 layer employed in the G-cell. To achieve a higher stability of the dye and thus reliable reproducibility the measurements were carried out in ultra-high-vacuum. A solvent environment is not expected to interfere with electron

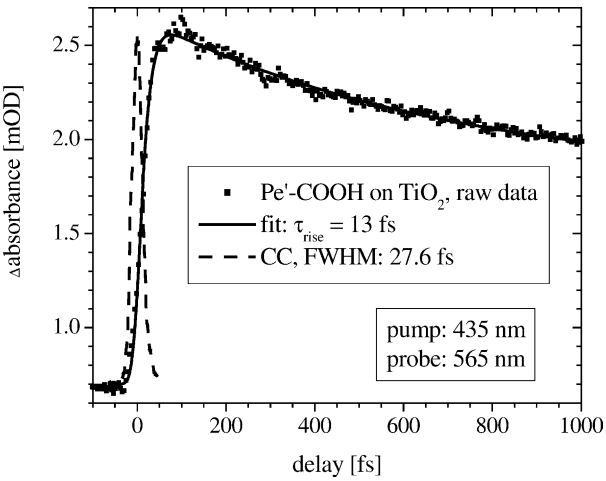

Fig. 1. Time resolved measurement of electron transfer from the excited singlet state of the chromophore perylene bonded via a carboxyl group with close to perpendicular orientation of its long axis on the surface of anatase TiO_2.

transfer taking place on such a short time scale. Pump and probe pulse were described already in the Experimental section. Fig. 1 shows in addition the cross correlation function for this measurement. The signal in Fig. 1 rises with 13 fs time constant. The initial recombination is much slower and controls the decay of the signals shown in Fig. 1. It involves either the injected electron or an electron already present in the nm-size TiO_2 particle. It will be shown elsewhere that the excited singlet state of perylene decays in this system with identical time constant of 13 fs as measured in the rise of the cation in Fig. 1. Thus, the electron injection time is 13 fs from the excited singlet state of the chromophore perylene attached via one carboxyl group with its long axis oriented in close to perpendicular direction with respect to the surface of anatase TiO_2 [26]. Apart from the distance dependence the injection time can depend also on the orientation and on the size of the chromophore. It is, however, not easy to see why electron transfer from the bypiridil ligand in the case of the N3 dye should occur with a time constant longer than the 13 fs measured for perylene when both are bonded to TiO_2 via a carboxylic group.

One of the virtues of investigating systems in ultra-high-vacuum is experimental access to the relative positions of the energy levels in the system. The experimental data is shown in Fig. 2 as UPS difference spectrum measured with respect to the Fermi level in the sponge-like anatase TiO_2 layer. The two peaks at the left in Fig. 2 are the first two ionization energies of perylene bonded via the carboxyl group to the surface of nm-structured anatase TiO_2. The first peak in the excitation spectrum, with 2.7 eV for the 0.0 energy of the transition to the first excited singlet state, was added to the highest ionization energy (HOMO) to yield the third peak shown at the right. The latter illustrates the energy of the electron injecting orbital of the excited singlet state with respect to the Fermi level in the TiO_2 layer. The latter was

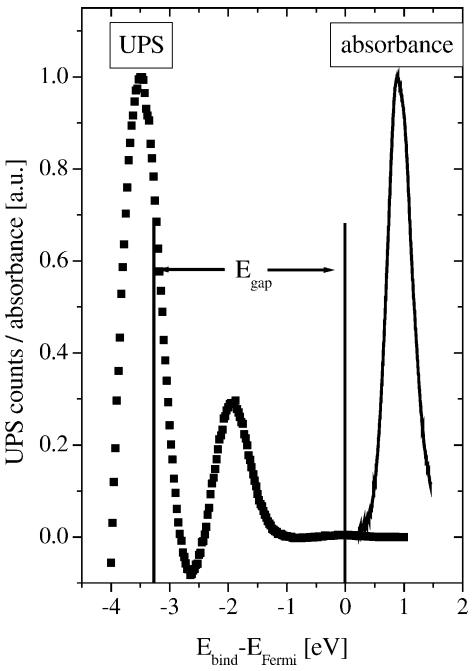

Fig. 2. UPS difference spectrum showing the ground state energy, peak in the center, and the first excited singlet state energy, peak to the right, of the chromophore perylene relative to the Fermi level in sponge-like nm-structured anatase TiO_2 where the chromophore perylene was attached via a carboxyl group.

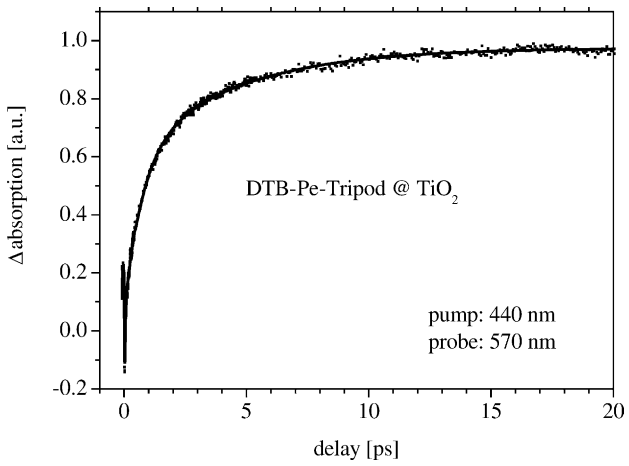

Fig. 3. Rise of the perylene cation absorption after generating the first excited singlet state of perylene anchored with a long tripod-type anchor-cum-spacer group on anatase TiO_2.

located close to the lower edge of the conduction band of TiO_2 in this respective preparation. It is clear from Fig. 2 that the electron injecting orbital is located roughly 1 eV above the lower edge of the conduction band. This makes a sufficiently wide energy range of unoccupied electronic levels in TiO_2 available for electron injection from the first excited singlet state of perylene.

Combining the information gained from Figs. 1 and 2 one can infer that the so-called wide band limit [25] for electron injection is realized in this system. In the latter case all the Franck-Condon factors of the electron transfer reaction are available in parallel and thus electron transfer is controlled only by the electronic coupling strength between the donor orbital and the electron accepting wavefunctions in TiO_2. The electron injection time of 13 fs corresponds to injection dynamics where most nuclear modes are comparatively slow such that they can neither precede nor accompany electron transfer. Thus, very little deviation can occur from the ground state nuclear coordinates of perylene prior to light-induced electron transfer in this system. In general, heterogeneous electron transfer can make use sequentially of several curve crossing points [21,25,27]. In summary, heterogeneous electron transfer dynamics can be very different in this system from electron transfer dynamics described by the well-known Marcus–Gerischer–Jortner scenario of non-adiabatic electron transfer between molecular donors and acceptors [9]. Making use of the measured 13 fs injection time and the fact that electron transfer is controlled here only by the electronic coupling strength one can infer that the electronic coupling strength is 50 meV in this system. We will defer the discussion of how much direct optical charge transfer is connected with such a short electron transfer time to a later paper. The increase in the electron transfer time with increasing distance can be seen in Fig. 3. The much longer rise time of 3.8 ps can be seen for the same perylene cation since the rim of the chromophore was attached via a long rigid tripod anchor-cum-spacer group [20] at a distance of about 1 nm from the TiO_2 surface. The long axis of perylene was again oriented close to perpendicular with respect to the surface of anatase TiO_2.

One can see additional shorter electron injection time constants in Fig. 3. The latter are attributed to adsorption sites where the perylene chromophore had come close to a TiO_2 wall in the nm-structured layer such that the distance was much shorter than the 1 nm distance realized with the tripod structure mounted on a planar surface. We are interested here only in the electron transfer time for the latter ideal adsorption configuration.

From the very short, 13 fs, and the very long, 3.8 ps, time constants of electron transfer over a very short, i.e. about 0.3 nm, and a very long, i.e. about 1 nm, distance, respectively, one can draw the following conclusions with respect to the G-cell. It is clear that primary electron transfer must occur fast compared to the time scale of any competing reaction or deactivation path. As will be discussed further, it is important for maintaining an acceptable conversion efficiency close to 10% in the G-cell that the ionized chromophore is reduced also fast enough by reduced redox ions and return by this path to the ground state prior to any recombination reaction. It is equally important for the efficiency of the G-cell that the corresponding oxidized species generated in this reaction react only very slowly with the electrons injected into the TiO_2 layer. Hitherto these two requirements can be met best with suitable redox ions, i.e. the I^-/I_3^- couple, in a solvent environment. Reorganization of the solvent

environment upon electron transfer introduces, however, additional small Franck-Condon factors into the electron transfer dynamics [9]. The latter can slow down considerably an electron transfer reaction with a large reaction distance, e.g. that shown in Fig. 3. For dyes like N3 with fast decay to a lower excited state such a slow electron transfer from a large distance would drastically lower the injection efficiency in the G-cell. Unfortunately, at present it is not yet clear whether the energetic position of the N3 dye on the surface of TiO_2 fulfills the above mentioned wide band limit criteria. Because of additional open questions raised above a conclusive assessment is not yet possible of the electron transfer dynamics for the N3 dye on the nm-structured anatase TiO_2 layer of the G-cell. It is clear, however, that only the very close contact between the donor orbital of the chromophore and the electronic acceptor states of the semiconductor together with a strong chemical bond facilitated by a short anchor group can eliminate most of the undesired slowing down effect of the solvent. Binding the N3 in this way to the TiO_2 surface one can utilize the solvent as a medium that accommodates suitable redox ions without slowing down the electron injection time. Thus, forming a short chemical bond between the ligand of the ruthenium-dye and the surface of TiO_2 is an excellent idea [1,18]. The experimental result described above for perylene suggests that the corresponding electron transfer time for the electron located on the bipyridil ligand of the N3 dye that is bonded via the carboxyl group to TiO_2 should also be of the order of 13 fs or shorter, in agreement with our earlier experimental estimate [11]. Three important features are nicely realized at the same time in the G-cell [1,18], firstly ultrafast primary charge separation, secondly fairly fast consecutive reduction of the oxidized state via a suitable redox ion in solution, and thirdly extremely slow recombination with the oxidized state of the redox ion. Efforts made by several groups over the last years of circumventing one of these three critical features of the G-cell have not been really successful. It is clear from the above discussion that a simpler dye would be preferable over the complicated situation encountered with the N3 dye. The situation would be much simpler if the electron could be lifted to only one electronic donor orbital that is coupled directly via a short anchor group to the acceptor states of the semiconductor. Corresponding dyes have been synthesized recently but it is not clear yet whether they can meet the other requirements of firstly covering the visible spectrum with a sufficient oscillator strength for absorption of the sunlight, secondly achieving a sufficiently dense packing on the inner surface of the sponge-like nm-structured TiO_2 layer, and thirdly providing a sufficiently fast electron injection reaction. It will be shown below that transport of injected electrons in the nm-structured TiO_2 layer is so slow that in spite of very slow recombination one cannot increase the thickness of the nm-structured TiO_2/electrolyte layer in the G-cell. Otherwise there would be higher recombination losses during the longer transport from the outskirts of a thicker layer.

4. Model for photocurrent transients in the G-cell

In many different experiments it has been found that transport of the photo-injected electrons in the nm-structured TiO_2/electrolyte layer can be described to a good approximation as diffusive motion where the effective diffusion constant varies with the degree of trap filling. The diffusion equation with appropriate boundary conditions has been applied successfully for describing firstly the photocurrent excitation spectrum [28], secondly photo-impedance measurements [29], and thirdly admittance measurements [5,6]. The dielectric response of the highly conductive electrolyte screens the photo-injected excess electrons in the nm-size TiO_2 colloids that make up the transport layer [4,30]. Due to the much higher conductance in the electrolyte phase, the assumption of unipolar diffusion of electrons in the TiO_2 phase appears to work well [31]. The response of the ions in the surrounding electrolyte to primary charge separation in the G-cell is assumed fast enough for neglecting it in the description of transport processes that occur on a much slower time scale. We apply here the above model of diffusive motion for describing photocurrent transients that are generated in the G-cell by exposing it to fairly short laser pulses. Transport of the screened electrons through the nm-structured TiO_2/electrolyte layer is described as time dependent diffusion, where the generation of electrons is introduced as the source term, recombination as the lifetime. A corresponding physical model is embedded as the generalized current source term into the equivalent circuit shown in Fig. 4. The resistance and capacitance in the latter represent the overall resistive and capacitive behavior of the G-cell. The current source term $j_s(t)$ charges the capacitive element C and creates a voltage drop in the series resistance R of the G-cell.

The external circuit adds the additional series resistance R_e. The capacitive element C is located close to the highly conductive SnO_2 electrode onto which the colloidal TiO_2 was deposited. The physical origin of the capacitive element

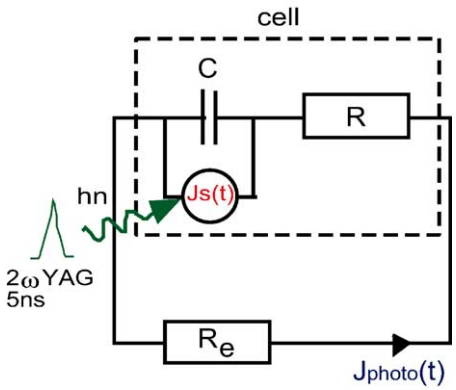

Fig. 4. Equivalent circuit representing the resistive and capacitive behavior of the G-cell with an external load R_e. The current source $j_s(t)$ is derived from a diffusion model with source term, lifetime, and appropriate boundary condition for charge separation.

has been explained earlier [4]. It is created at the interface during the formation of the contact of two different materials. In contrast to a bulk semiconductor electrode, where the space charge capacitance usually extends over several hundred nanometers, the highly conducting electrolyte surrounds every nm-size TiO_2 particle in the sponge-like TiO_2 network. This leads to a screening effect and contracts also the width of the space charge layer near the planar SnO_2 electrode to the range of a few TiO_2 colloidal diameters [4]. The latter is on average in the range of 20 nm. In this idealized picture, transport of the screened photo-generated excess charge $n(x, t)$ in the nm-TiO_2 network can be described by the diffusion equation, with the possible exception of the region very close to the SnO_2 substrate as will be discussed below.

$$\frac{\partial n(x,\ t)}{\partial t} = D\frac{\partial^2 n(x,t)}{\partial x^2} - \frac{n(x,t)}{\tau} + \begin{cases} \alpha\eta\, I_0(t)\, \mathrm{e}^{-\alpha x} \text{ (SE case)} \\ \alpha\eta\, I_0(t)\, \mathrm{e}^{-\alpha(L-x)} \text{ (EE case)} \end{cases} \quad (1)$$

D is equal to diffusion coefficient, τ the lifetime, α the absorption coefficient, L the thickness of the TiO_2 film, η the quantum yield of excess electron generation, and $I_0(t)$ the temporal excitation profile. The 'SE case' refers to illumination through the SnO_2/TiO_2 interface and the 'EE case' to illumination through the SnO_2/electrolyte interface [14]. At the macroscopic boundary between the sponge-like TiO_2 layer and the compartment filled only by electrolyte ($x = L$), it is assumed that the screened electrons are reflected back into the sponge-like TiO_2 layer. At the opposite boundary of the TiO_2 layer with the n-SnO_2 electrode ($x = 0$), it is assumed that the electrons are separated from their screening and counter charge and are thus contributing to the photocurrent. These two different assumptions are represented by the following boundary conditions:

$$\frac{\partial n(L,t)}{\partial x} = 0\,|_{x=L}\ ,\ k_{\mathrm{es}}\, n(0,t) = D\frac{\partial n(0,t)}{\partial x}\bigg|_{x=0} \quad (2)$$

k_{es} [cm/s] = velocity at the SnO_2/TiO_2 interface for the disappearance of excess electrons from the sponge-like TiO_2 layer. This type of boundary condition does not distinguish between the contribution of the excess electrons to the photocurrent and their recombination at the interface, e.g. with oxidized redox ions or holes. Assuming that recombination at the interface can be neglected one can describe the photocurrent at $x = 0$ as follows:

$$j_{\mathrm{s}}(t) = \mathrm{e}(k_{\mathrm{es}} n(0,\ t) + \gamma\, I_0(t)) = \mathrm{e}\left(D\frac{\partial n(0,t)}{\partial x}\,|_{x=0} + \gamma\, I_0(t)\right) \quad (3)$$

For the simulations a Gaussian pulse profile has been used for the source term $I_0(t)$. There is an additional source term $\gamma^* I_0(t)$ in Eq. (3). It represents charge generation in the spatial range of the space charge capacitor (see Fig. 4) where it is assumed that electrons are rapidly driven to the SnO_2 electrode by the action of an electric dark equilibrium field. The corresponding current source term should be shorter than the time resolution of the experiment. Hence it is assumed that this current source term has the time profile of the laser pulse $I_0(t)$. For $\gamma = 0$ the photocurrent $j_{\mathrm{s}}(t)$ should show a clean diffusion like time behavior. There is no analytical solution to Eq. (1) for this type of generation term. Numerical solutions to Eqs. (1) and (3) were obtained by applying the Press et al. [32] discretisation scheme on a non-uniform logarithmic time mesh. In order to obtain the tabulated solution for $j_{\mathrm{s}}(t)$ for every value of t, cubic spline interpolation has been used. The current flowing in the external circuit $J_{\mathrm{photo}}(t)$ (Fig. 4) was then obtained by solving the ordinary differential equation corresponding to the equivalent circuit shown in Fig. 4 with the interpolated current source term $j_{\mathrm{s}}(t)$. For calculations with a logarithmic time mesh over a range of six decades an algorithm with adaptive step size control (LSODE) was used [33].

5. Experimental and simulated photocurrent-transients

The use of two transparent conducting electrodes in the G-cell makes it possible to illuminate the cell from opposite directions. A different charge carrier generation profile can be obtained, e.g. with respect to the SnO_2 contact, for the two different directions of illumination provided the optical density of the dye-loaded sponge-like TiO_2 layer is sufficiently high at the respective wavelength. The two different situations are illustrated in Fig. 5. Two typical measured photocurrent transients are also shown for a laser pulse of 533 nm wavelength. It should be noticed that two separate consecutive peaks appeared in the photocurrent transient when the laser pulse entered the G-cell through the SnO_2 electrode shown at the right that is in contact with the electrolyte compartment (EE case). Illumination from the opposite direction, i.e. through the other SnO_2 electrode that is in direct contact with the TiO_2 layer (SE case), is also illustrated in Fig. 5. The transients shown in Fig. 5 are normalized with respect to the height of the first photocurrent peak. The SE photocurrent transient decayed continuously after having reached the first peak with non-exponential behavior lasting into the ms time range. The photocurrent for illumination from the other direction (EE case) was strikingly different. In addition to the first peak as observed for the SE case there was a second delayed peak of the photocurrent in the EE case that occurred long after the first peak (Fig. 5). The average transport time for electrons to reach the SnO_2 electrode in contact with the TiO_2 layer was longer for the EE illumination case compared to the SE case. The crucial final separation of opposite charges occurs in the G-cell at the latter interface. Correspondingly, the delayed second peak occurred only with EE illumination. Lindquist's group [14] has studied the origin of the delayed peak in some detail by

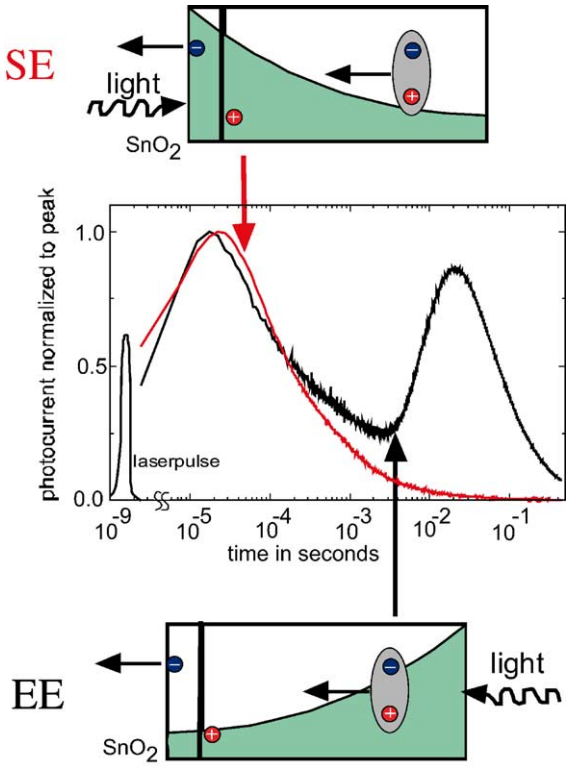

Fig. 5. Upper panel: initial spatial distribution of photo-generated electrons in the G-cell for laser pulse illumination through the SnO_2 electrode (SE illumination). Center panel: two typical measured photocurrrent transients for SE vs. EE illumination. Lower panel: initial spatial distribution of photo-generated electrons in the G-cell for laser pulse illumination through the electrolyte space (EE illumination). Two consecutive peaks can be seen in the photocurrent transient (center panel) for the EE case but not for the SE case.

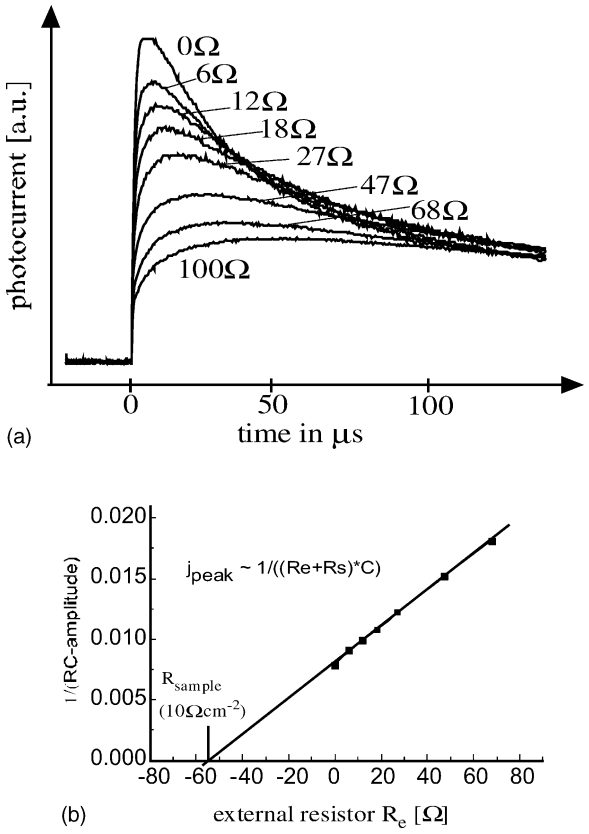

Fig. 6. (a) First peak of the measured photocurrent transients for different values of the external resistor R_e given as parameter value at the respecitve curve. (b) Plot of the magnitude of the measured first photocurrent peak (indicated at the abscissa as 1/*RC*-amplitude) for different values of the external resistor R_e vs. the value of R_e for the respective measured photocurrent peak value

investigating transport through dye-loaded TiO_2/electrolyte layers of different thickness. These authors have attributed the delayed second peak to diffusive motion of electrons to the SnO_2 electrode that is in direct contact with the TiO_2 layer. Our group has reported already briefly on the first peak arising in the μs time range and has explained its origin [5]. As can be seen in Fig. 5 the shape of the first peak was almost identical for the two different directions of illumination. In contrast, the occurrence of the delayed peak only for EE illumination but not for SE illumination leads to a strikingly different behavior of the two different photocurrent transients in the ms time range (Fig. 5). The shape of the first peak was the same for EE and SE illumination but its magnitude was much higher for SE illumination. Note that under EE illumination the second delayed peak contributed about 99% to the total photocurrent and the first peak only 1%. Fig. 4 shows that the *RC* behavior of the G-cell can be tested and its capacitance *C* can be determined by measuring the photocurrent transients for different values of the external resistance R_e. The corresponding photocurrent transients are shown in Fig. 6a in the relevant time window. In later time windows, not shown in Fig. 6a, the transients were not affected by the change in the value of the series resistance R_e. For the same G-cell there was no significant difference noticeable in the *RC* behavior of the first peak in the case of EE and SE illumination. There were, however, significant differences in the *RC* times measured at different G-cells. Apparently, our preparation procedure was not sufficiently standardized. When subjected to *RC* shaping (Fig. 5) the height of the early photocurrent peak should be proportional to $1/(RC)$, where R is the total series resistance. The result from such measurements is shown in Fig. 6b where the measured peak height is plotted versus the value of the external series resistance R_e. Extrapolation to $j_{peak} = 0$ yields the intrinsic series resistance $R_s = 10\,\Omega/cm^2$ for this G-cell. This value was in good agreement with the value obtained from dark current *I–V* measurements that were carried out with this G-cell. The capacitance of the cell was now obtained from the time constant for the decay of the first peak in the μs time window ($t = RC$). The value $C = 4$ $\mu F/cm^2$ was found for the capacitance of this G-cell. Typical values for several preparations of the G-cell fell into the range between 200 and 5 $\mu F/cm^2$. The latter experimental values are compatible with our simple model for the space charge capacitance in the G-cell [4]. Larger variations between different G-cells can be related to different concentrations of voids occurring in the TiO_2 layer near the SnO_2

electrode (substrate). Two extreme values for the capacitance should arise. Firstly, several μF/cm^2 are expected for the Helmholtz capacitance corresponding to the bare SnO_2 electrode in contact with only the electrolyte. Secondly, a much smaller capacitance is expected for the SnO_2 electrode covered by a solid layer of TiO_2. To check on this conjecture, SnO_2 electrodes were covered via spray pyrolysis with a thin (20 nm) dense layer of TiO_2 and the sponge-like TiO_2 layer was deposited on top of this thin solid layer of TiO_2. As expected, the corresponding G-cells showed much smaller values for the capacitance (200 nF/cm^2). The strong dependence of the measured *RC* time constant on the density of the TiO_2 layer on top of the SnO_2 electrode shows that the value of the capacitance at the TiO_2/SnO_2 interface is indeed controlling the capacitive behavior of the photocurrent transient. The measured photocurrent transients do not address other capacitive elements that arise in the G-cell for example at the SnO_2 counter electrode in contact with the electrolyte compartment.

Fig. 7 shows simulated photocurrent transients with a behavior closely resembling that of the experimental signals in the case of EE and SE illumination (Fig. 5). A change in the series resistance in the simulation (Fig. 8) yields good qualitative agreement with the corresponding behavior of the measured photocurrent transients (Fig. 6). To minimize the computational load, the temporal width of the electron generating function $g(x, t)$ was chosen longer (100 ns) than the actual duration of the laser pulse in the experiments (15 ns) but still short enough for keeping the rise time of the simulated transient unaffected. In the calculated transients (Figs. 7 and 8) the duration of the electron generating function $g(x, t)$ is shorter than both the *RC*-time and the diffusion time constants. The rise time of the first peak in the photocurrent transient is determined by the initial stage

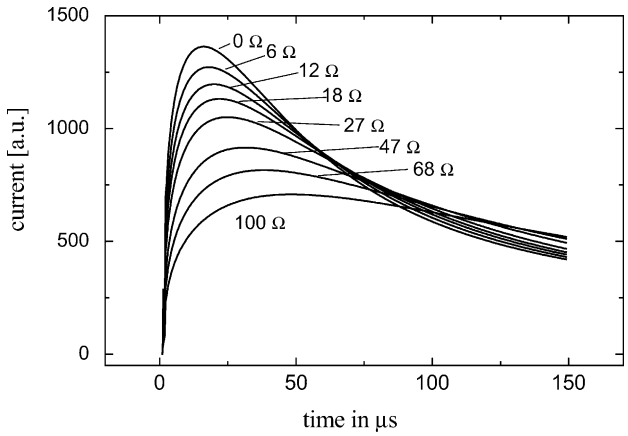

Fig. 8. Simulated photocurrent transients for different values of the external resistor R_e. Same parameter values as in Fig. 7, except for R_e assuming values between 0 and 100 Ω indicated at the respective curve.

of the diffusion controlled charging of the space charge capacitance *C*. The occurrence of two consecutive peaks is unique to the EE illumination direction for the case of a non-homogenous charge generation profile. The first peak did not show up in the earlier model calculations presented by the Lindquist group [14]. Three conditions must be met for this early peak to arise. Firstly, the *RC* time constant of the cell has to be shorter than the time scale for electron diffusion in the G-cell. With a typical *RC* time constant of about 100 μs, this condition is usually fulfilled at all operating conditions for the G-cell. Secondly, the generation rate at the back electrode, i.e. at the interface SnO_2/TiO_2 (compare Eq. (1), $x = 0$), must be sufficiently high. For $\alpha L \gg 1$ the initial concentration of photo-generated electrons at the back electrode and thus the generation rate at $x = 0$ becomes negligible, and the first peak smears out into

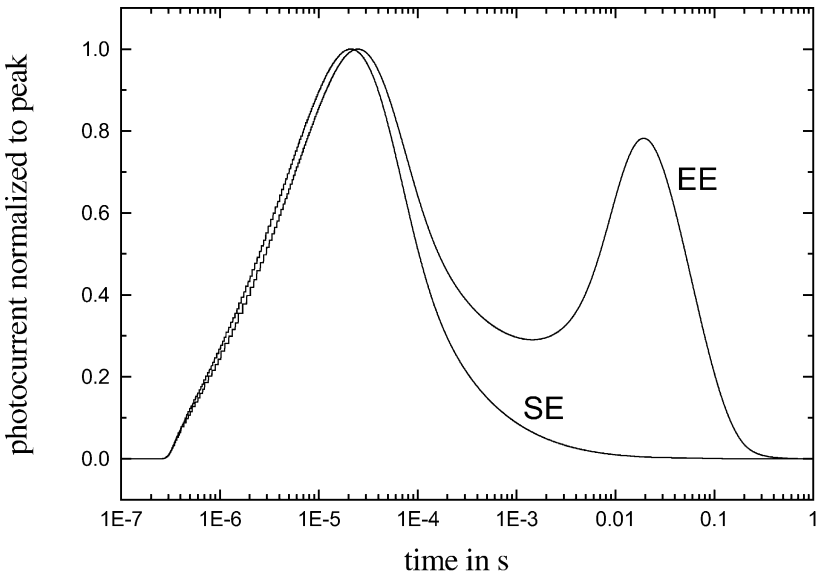

Fig. 7. Simulated photocurrent transients for EE and SE incidence of the laser pulse. Curves are normalized at the maximum amplitude. Parameters: $D = 2 \times 10^{-6}$ cm^2/s, $L = 5.4$ μm, $\alpha = 8 \times 10^3$ cm^{-1}, $\tau = 1$ s, $k_{es} = 100$ cm/s, $C = 500$ nF, $R = 50$ Ω, Re = 0 Ω, width of Gauss pulse = 500 ns FWHM.

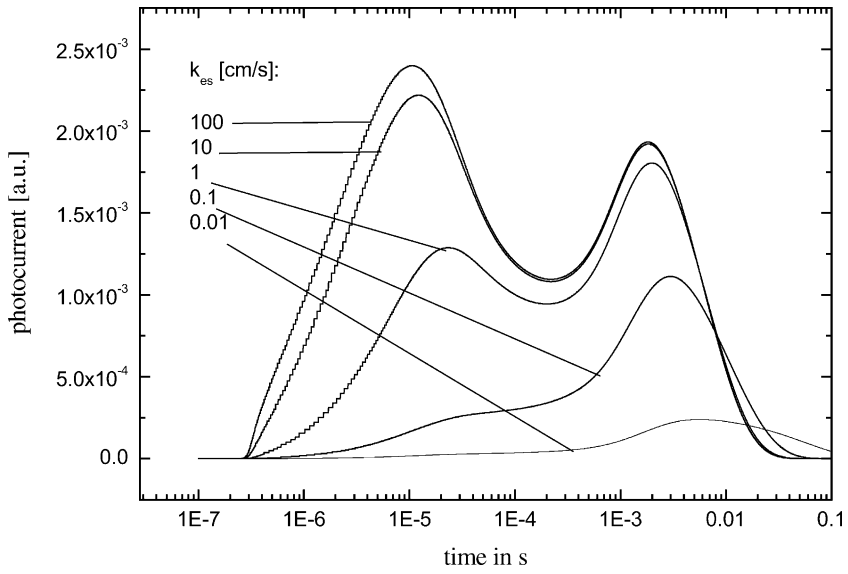

Fig. 9. Simulated photocurrent transients for different values of k_{es}, otherwise same parameter values as for Fig. 7.

a slowly rising current. When the generation rate becomes homogenous throughout the film ($\alpha L \ll 1$) the shapes of the photocurrent transients become very similar for both directions SE and EE of the impinging laser pulse. In this case the shape of both the photocurrent transients is similar to that shown already for illumination from the SE direction (Fig. 5). Thirdly, charge separation at the SnO_2/TiO_2 interface has to be faster than diffusion of the electrons through the TiO_2 network. The latter condition requires a high value for k_{es}, i.e. the velocity for charge separation or more generally for the disappearance of the screened electrons at this interface. To such a situation is usually referred to as 'diffusion limited' photocurrent. Transients simulated for different values of k_{es} are shown in Fig. 9. With all the other parameter values kept constant, a decrease in the value for k_{es} decreases the height of the first peak in the photocurrent transient. The quantum yield of the photocurrent drops significantly if k_{es} reaches values smaller than 10 cm/s. It was assumed up to here that k_{es} describes only charge separation and not quenching at the interface.

A different assumption can of course be easily introduced into the model. A high value for k_{es} can describe also fast recombination at the SnO_2/TiO_2 interface. The latter assumption is not valid, however, for the G-cell since the measured quantum yield of the photocurrent is very high at short-circuit conditions. So far, it was shown here that the principle features of the measured photocurrent transients are well reproduced by the above diffusion/capacitance model. This result is somewhat surprising when one considers also the highly non-linear behavior measured for the transport of screened electrons through the nm-structured TiO_2 network. The non-linear behavior arises from trap filling [15]and recombination [13] of the electrons in the layer addressed here for brevity mostly as TiO_2 layer that is actually the sponge-like nm-structured TiO_2 network filled with electrolyte. For impedance measurements the small signal approximation with linear transport equations is a good approximation. For describing photocurrent transients such an approximation is usually not a-priori justified. A more detailed model should consider the dependence of the transients on photon density and also on electric fields, including an external bias. Both effects are neglected in the present simulations.

6. Final charge separation in the G-cell

Final charge separation and recombination at the SnO_2/TiO_2 interface is accounted for in the model only by the same constant k_{es} in the boundary condition (Eq. (3)). A closer look at the initial rising part of the transients reveals a significant difference between the experimental and the simulated transients (Fig. 10). The dashed curve in Fig. 10 shows the rising part of a calculated transient for the diffusion/capacitance model considered so far. The experimental rise was much faster and could not be fitted with any set of parameter values using the above model. By increasing the diffusion constant the rise can be made faster in the simulation but then the slower part of the experimental transient shows a strong deviation from the calculated curve. Even if this deviation is ignored, one can still not obtain a good match with the experimental rise on the basis of the above diffusion model alone. At this point it is important to note that the much faster rise of the measured photocurrent compared to the simulation varied from sample to sample, it was not an artifact introduced by the measuring procedure. A close to perfect match with the experimental transient is obtained, however, when an additional fast current term is added to the simulation (solid curve in Fig. 10). For this additional current the assumption was made that it follows

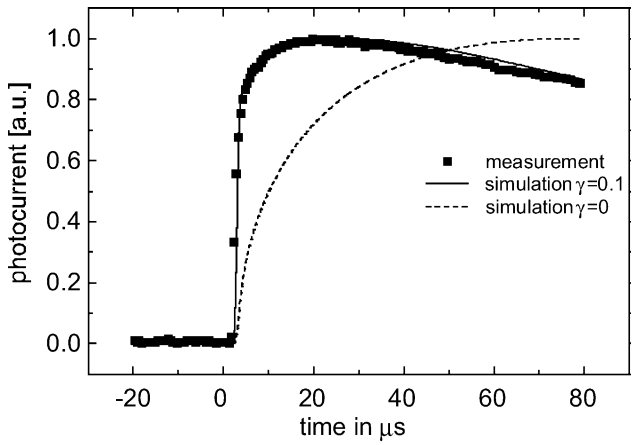

Fig. 10. Comparison of the experimental rise of the first peak of the photocurrent transient (solid squares) with a transient simulated with the diffusion model (dashed curve). Adding an instantaneous contribution to the photocurrent transient simulated with the diffusion model (solid curve) results in a perfect match with the experimental data.

the time profile of the generating laser pulse according to Eq. (3). It appears likely that this fast contribution arises due to different structural properties of the TiO_2 layer close to the SnO_2 electrode compared to the bulk of the layer. Close to the contact nm-particles could be packed more densely in the TiO_2 layer than in the rest of the layer and this could be connected with faster transport for the electrons. In the simulation this would correspond to a higher value for the diffusion coefficient near the SnO_2 electrode. A second possibility is faster electron transport due to an electric field near the interface. The latter could be set up in the dark when equilibrium is established at the interface of the two different materials. Such a situation is usually encountered at other types of hetero-junctions. Except for slightly different boundary conditions and different transport parameters the model applied here is the same that was used earlier for modeling photocurrent transients at the c-Si-liquid junction [34]. The fast disappearance of the screened electrons at the SnO_2/TiO_2 interface is due to the fast transfer of the electrons into the SnO_2 electrode and not to recombination losses at the interface. The latter conclusion is drawn considering firstly the high value of k_{es} required here in the simulation to match the experimental data and secondly the measured high photocurrent quantum yield. On the basis of the present experimental data it cannot be decided whether this fast charge separation process is controlled by a corresponding equilibrium dark potential or by a suitable band offset at the interface, or both. Recent experimental data suggest that an equilibrium electric field is likely to be present at the interface [17]. The question whether an equilibrium dark electric field is required for a successful operation of the dye cell has stimulated a long debate in the past. The main reason for the difficulty in answering this question for the G-cell is the extremely long lifetime of the photo-generated electrons in the mixed electrolyte/TiO_2 layer. The long lifetime is achieved in the G-cell due to very slow recombination with the oxidized species of the redox couple, i.e. I_3^-, and by a suitable choice of supporting electrolyte. It is clear that an equilibrium electric field at the interface represents the easiest and most efficient way of realizing fast transfer of the electrons across the interface. As long as the lifetime of the electrons is sufficiently long, however, such a fast transfer is not strictly required. A fairly slow interfacial charge separation would increase the stationary concentration of the minority carriers in the device. Thus, the recombination rate would increase since it is given by the minority carrier concentration dived by the minority carrier lifetime. A good efficiency of the cell can be expected if the recombination rate is much smaller than the generation rate of minority carriers for a large part of the current voltage curve. Otherwise a poor fill factor is obtained. We have carried out device simulations comparing two p–n hetero-junctions. Band gaps and transport properties were chosen as to resemble the situation in the G-cell. By changing the electron affinity of one of the materials it is possible to create two different energetic situations, i.e. band offsets, at the interface with otherwise identical parameter sets. One device had a negligible equilibrium electric field and just a band offset at the interface. The other device had two different Fermi levels in the two materials prior to equilibration and thus after equilibration a strong band bending at the interface. Both devices showed a similar performance in the simulations, i.e. 5 and 6% solar conversion efficiency and identical open circuit voltage, provided the minority carrier lifetime in the light-absorbing layer was chosen longer than 100 ms. The performance of both the devices deteriorated when the minority carrier lifetime was lowered. The performance of the device without built-in electric field degraded, however, much stronger than that of the device with the built-in electric field. At 0.1 ms lifetime the field-driven device still kept the efficiency higher than 1%, whereas the device without electric field dropped the efficiency to below 0.1%. Most of the degradation was caused by the decreasing fill factor, whereas the open circuit voltage remained almost unaffected. The above simulations demonstrate the importance of a built-in electric field at the interface at least for a light-absorbing layer that does not provide an extraordinary long lifetime for the minority carriers. It is likely that the latter condition is the most difficult target to meet when trying to match the performance of the G-cell with a similarly constructed true solid state type solar cell.

7. Summary

A time constant of 13 fs was measured via transient absorption for electron transfer from the excited singlet state of the chromophore perylene when bonded via a carboxyl group to anatase TiO_2. A similar time constant can be inferred for primary charge separation in the Grätzel-cell from the bipyridil ligand of the so-called N3 ruthenium dye into

anatase TiO_2. At a distance of about 1.3 nm, realized with a tripod spacer-cum-anchor group, the electron transfer time from the perylene chromophore became much longer, i.e. 3.8 ps. In the presence of a solvent further slowing-down of the electron transfer is expected to occur due to additional Franck-Condon factors. Thus, anchoring the electron injecting chromophore with a short anchor group, e.g. the carboxyl group, is an essential requirement for fast injection and high current yield. This feature has been incorporated already into the first version of the Grätzel-cell. Laser pulse induced transients of the photocurrent were measured for illumination firstly through the SnO_2/TiO_2 interface (SE) and secondly through the opposite SnO_2/electrolyte interface (EE). For EE illumination the transient showed two peaks, the first in the μs range and the second in the ms range, whereas only the early peak occurred in the case of SE illumination. The different shapes of EE compared to SE transients were easily explained by employing a time dependent diffusion equation with appropriate boundary conditions. The rise to the first peak was faster than diffusion controlled if the same diffusion constant was assumed near the interface as was measured in the bulk of the nm-structured sponge-type TiO_2/electrolyte layer. To account for the fast rise of the photocurrent either a higher diffusion coefficient must be valid near the SnO_2/TiO_2 interface or final charge separation is driven by an equilibrium electric field near the interface. A model calculation was performed for the photovoltaic action of a hetero-junction in the absence and in the presence of an electric field. For the case of recombination losses the simulation showed a higher solar conversion efficiency if final charge separation was driven by an electric field compared to charge separation supported by only a down-hill band off-set.

References

[1] M. Grätzel, B. ÓRegan, Nature 353 (1991) 737.
[2] P. Würfel, Physik der Solarzellen, Spektrum Akademischer Verlag, Heidelberg, 1995, p. 92.
[3] R.T. Ross, T.L. Hsiao, J. Appl. Phys. 48 (1977) 4783.
[4] K. Schwarzburg, F. Willig, J. Phys. Chem. B 103 (1999) 5743.
[5] K. Schwarzburg, F. Willig, J. Phys. Chem. B 107 (2003) 3552.
[6] G. Kron, T. Egerter, J.H. Werner, U. Rau, J. Phys. Chem. B 107 (2003) 3556.
[7] P. Würfel, T. Trupke, Physik J. 2 (2003) 45.
[8] S.R. Kurtz, J.M. Olson, A. Kibbler, in: Proceedings of the 21st IEEE PVSC, Orlando, 1990, p. 138.
[9] R.A. Marcus, N. Sutin, Biochim. Biophys. Acta 811 (1985) 265; R.A. Marcus, J. Phys. Chem. 94 (1990) 1050.
[10] V. Shklover, M.-K. Nazeeruddin, S.M. Zakeeruddin, C. Barbé, A. Kay, T. Haibach, W. Steurer, R. Hermann, H.-U. Nissen, M. Grätzel, Chem. Mat. 9 (1997) 430.
[11] T. Hannappel, B. Burfeindt, W. Storck, F. Willig, J. Phys. Chem. B 101 (1997) 6799.
[12] S.A. Haque, Y. Tachibana, R.L. Willis, J.E. Moser, M. Grätzel, D.R. Klug, J. Durrant, J. Phys. Chem. B 104 (2000) 538; J. Nelson, S.A. Haque, D.R. Klug, J. Durrant, Phys. Rev. B 63 (2001) 205321.
[13] L.M. Peter, N.W. Duffy, R.L. Wang, K.G.U. Wijayantha, J. Electroanal. Chem. 524 (2002) 127.
[14] A. Solbrand, H. Lindström, H. Rensmo, A. Hagfeldt, S.-E. Lindquist, S. Södergren, J. Phys. Chem. B 101 (1997) 2514; A. Solbrand, A. Henningsson, S. Södergren, H. Lindström, A. Hagfeldt, S.-E. Lindquist, J. Phys. Chem. B 103 (1999) 1078.
[15] K. Schwarzburg, F. Willig, Appl. Phys. Lett. 58 (1990) 2520. The results in this paper were obtained with the highly structured TiO_2/electrolyte layer prepared from an oxidized Ti-sheet (Augustinski-Grätzel type TiO_2 electrodes). Our results obtained slightly later with the nm-structured TiO_2/electrolyte layer (kindly supplied by P. Liska and M. Grätzel) were identical to the results published in this paper except for the “fast initial transport” now being absent in the latter type of layer..
[16] K. Schwarzburg, F. Willig, J. Phys. Chem. B 107 (2003) 13546.
[17] G. Kron, U. Rau, J.-H. Werner, J. Phys. Chem. B 107 (2003) 13258.
[18] M.K. Nazeeruddin, A. Kay, I. Rodicio, R. Humphrey-Baker, E. Müller, P. Liska, N. Vlachopoulos, M. Grätzel, J. Am. Chem. Soc. 115 (1993) 6382.
[19] R. Ernstorfer, L. Gundlach, S. Felber, W. Storck, R. Eichberger, F. Willig, submitted for publication.
[20] W. Guo, E. Galoppini, G. Rydja, G. Pardi, Tetrahedron Lett. 4 (2000) 7419.
[21] C. Zimmermann, F. Willig, S. Ramakrishna, B. Burfeindt, B. Pettinger, R. Eichberger, W. Storck, J. Phys. Chem. B 105 (2001) 9245.
[22] J. Piel, E. Riedle, L. Gundlach, R. Ernstorfer, R. Eichberger, unpublished.
[23] G. Benko, J. Kallinoinen, J.E.I. Korppi-Tommola, A.P. Yartsev, V. Sundstrom, J. Am. Chem. Soc. 124 (2002) 489.
[24] A.T. Yeh, C.V. Shank, J.K. McCusker, Science 289 (2000) 935.
[25] S. Ramakrishna, F. Willig, V. May, A. Knorr, J. Phys. Chem. B 107 (2003) 607; S. Ramakrishna, F. Willig, V. May, Phys. Rev. B 62 (2000) R16330.
[26] We are grateful to Dr. N. Petter Persson, Theoretical Chemistry, University of Uppsala, for suggesting a plausible adsorption configuration based on DFT data.
[27] W. Stier, O.V. Prezhdo, J. Phys. Chem. B 106 (2002) 8047.
[28] S. Södergren, A. Hagfeld, J. Olsson, S.-E. Lindquist, J. Phys. Chem. 98 (1994) 5552.
[29] L.M. Peter, E.A. Ponomarev, G. Franco, N.J. Shaw, Electrochim. Acta 45 (1999) 549.
[30] A. Zaban, A. Meier, B.A. Gregg, J. Phys. Chem. B 101 (1997) 7985.
[31] N. Kopidakis, E.A. Schiff, N.G. Park, J. van de Lagemaat, A.J. Frank, J. Phys. Chem. B 104 (2000) 3930.
[32] H.P. Press, S.A. Teukolsky, W.T. Vetterling, B.P. Flannery, Numerical Recipes in C, Cambridge University Press, Cambridge, 1992.
[33] G.D. Byrne, A.C. Hindsmarsh, J. Computat. Phys. 70 (1987) 1.
[34] K. Schwarzburg, F. Willig, J. Phys. Chem. B 101 (1997) 2451.